AIMS Biophysics

AIMS Biophysics, 10(1): 50–66.
DOI: 10.3934/biophy.2023005
Received: 04 September 2022
Revised: 23 October 2022
Accepted: 31 October 2022
Published: 30 January 2023

http://www.aimspress.com/journal/biophysics

Research article

Identification of potential SARS-CoV-2 papain-like protease inhibitors with the ability to interact with the catalytic triad

Murtala Muhammad[1,2,*], I. Y. Habib[3], Abdulmumin Yunusa[1], Tasiu A. Mikail[1], A. J. ALhassan[4], Ahed J. Alkhatib[5], Hamza Sule[6], Sagir Y. Ismail[1] and Dong Liu[2,*]

[1] Department of Biochemistry, Kano University of Science and Technology, Wudil, Nigeria
[2] College of Life Science, Hebei Normal University, 050024 Shijiazhuang, China
[3] Department of Chemistry, Sa'adatu Rimi College of Education Kumbotso, Kano, Nigeria
[4] Department of Biochemistry, Bayero University Kano, Nigeria
[5] Faculty of Medicine, Jordan University of Science and Technology, Jordan
[6] Department of Applied Medical Science, Bayero University, Kano, Nigeria

* **Correspondence:** Email: murtala19@yahoo.com, pqw1234@163.com; Tel: +2348138294220.

Abstract: Severe acute respiratory syndrome corona virus2 (SARS-CoV-2) is responsible for the current pandemic that led to so many deaths across the globe and still has no effective medication. One attractive target is Papain-like protease (PLpro), which plays a critical role in viral replication. Several important structural features dictate access to the PLpro narrow active site, which includes a series of loops surrounding the area. As such, it is difficult for chemical compounds to fit the SARS-CoV-2 PLpro active site. This work employed a computational study to discover inhibitors that could bind to the SARS-COV-2 PLpro active site, mainly by virtual screening, molecular dynamic simulation, MMPBSA and ADMET analysis. Eight potential inhibitors were identified: carbonoperoxoic acid, Chrysophanol-9-anthrone, Adrenolutin, 1-Dehydroprogesterone, Cholest-22-ene-21-ol, Cis-13-Octadecenoic acid, Hydroxycarbonate and 1-(4-(4-Methylphenyl)-5-phenyl-1,3-oxazol-2-yl) isoquinoline, with binding scores of −4.4, −6.7, −5.9, −6.7, −7.0, −4.6, −4.5 and −5.6 kcal/mol, respectively. All these compounds interacted with critical PLpro catalytic residues and showed stable conformation in molecular dynamics simulations with significant binding energies of −12.73 kcal/mol, −10.89 kcal/mol, −7.20 kcal/mol, −16.25 kcal/mol, −19.00 kcal/mol, −5.00 kcal/mol, −13.21 kcal/mol and −12.45 kcal/mol, respectively, as revealed by MMPBSA analysis. ADMET analysis also indicated that they are safe for drug development. In this study, we identified novel compounds that interacted with the key catalytic

residues of SARS-CoV-2 PLpro with the potential to be utilized for anti-Covid-19 drug development.

Keywords: SARS-CoV-2; PLpro; inhibitors; molecular docking; molecular dynamics simulations; MMPBSA

1. Introduction

Emerging and re-emerging infectious diseases remain among the greatest threats to human survival on this planet. Animal Pathogens mutate and evolve continuously, gaining the ability to become zoonotic or less susceptible to treatment [1].

Coronaviruses are enveloped RNA viruses distributed broadly among reptiles, mammals and birds, causing respiratory, enteric, hepatic and neurologic diseases. Recently, a severe human respiratory illness believed to be of animal origin has been responsible for several deaths across the globe [2–4]. The disease has been declared a global health emergency by the World Health Organization (WHO) [4]. Studies suggested that a new highly infectious strain of Coronavirus (SARS-CoV-2) is responsible for the pandemic [3]. So far, there is no globally accepted standard therapeutic for its management [2].

Papain-like protease (PLpro) is a coronavirus enzyme that plays an essential role in viral replication and pathogenesis. It converts viral polyprotein into a functional replicase complex [5]. PLpro exhibits deubiquitinating and deISG15ylating (interferon-induced gene 15) activities in SARS-CoV and MERS-CoVs [6–9]. The catalytic triad Cys111, His272 and Asp286 is located at the interface between the thumb and palm sub-domains of the enzyme [6,10,11]. Small chemical compounds and natural products are rich sources of lead compounds that could be explored for new drug development. With the recent advancement in computational chemistry, chemical libraries could be screened for compounds that could interact with biological structures and inhibit the proliferation and survival of pathogens [12–14]. Several scientists have screened various chemical libraries in an attempt to discover potent PLpro inhibitors. For instance, Alamri *etal.* identified three compounds from a library of more than six thousand protease inhibitors, Hajbabaie *etal.* screened more than thirty thousand compounds, Peng *etal.* identified four promising PLpro inhibitors from a 1.6 million compound library, and many other similar studies were reported with varying success stories [15,16]. Computational ligand-target prediction has proven reliable in drug discovery [7]. Recent in-vitro studies imply that Plpro inhibitors that bind to the active or ubiquitin-binding sites are promising candidates for drug development [6]. *C. occidentalis* was reported to have demonstrated remarkable ethnomedicinal properties such as antimicrobial activity, anti-viral properties, anti-carcinogenicity, anti-proliferation properties and antioxidant properties [17]. Therefore, the present study will utilize in silico techniques to identify potent Covid-19 PLpro inhibitors with the ability to interact with the PLpro catalytic residues from *C. occidentalis* phytochemicals National Cancer Institute (NCI) and PubChem chemical compounds databases for anti-COVID-19 drug development.

2. Materials and methods

2.1. Ligand retrieval and preparation

More than Fifty *C. occidentalis* phytochemicals were obtained from the literature [18,19], as

well as Six thousand chemical compounds from the NCI library (https://dtp.cancer.gov/) and PubChem (https://pubchem.ncbi.nlm.nih.gov/) databases, for the virtual screening. The NCI compounds employed in this study are NCI diversity set VI compounds tested in the NCI human tumor cell line screening, while the PubChem compounds were obtained from the PubChem similarity search of *C. occidentalis* phytochemicals that bind to the PLpro active site. The Ligands in SDF format were minimized and converted to PDBQT with PyRx-OpenBabel software.

2.2. Protein target preparation

The PDB structure of SARS-CoV-2 PLpro was retrieved from the Protein Data Bank (https://www.rcsb.org) (PDB ID: 7cmd). All hetero atoms were removed from the protein molecule using Discovery Studio software.

2.3. Molecular docking and docking validation

Molecular docking validation was conducted by re-docking the native ligand (GRL0617) of the 7cmd crystal structure to PLpro. Accordingly, GRL0617 was separated from the protein and prepared for docking using Discovery Studio (Version 20). The ligand was then docked back into PLpro's active site using Auto Dock Vina. The docked complex was superimposed with the X-ray resolved crystal Plpro (7cmd) bearing the co-crystallized ligand, and the root mean square deviation (RMSD) value was generated in PyMOL [20]. Site-directed docking around the PLpro active site was performed with all the Ligands. The receptor molecule remains rigid, and the ligands are flexible. Binding interactions were analyzed using Discovery Studio [21]. Only compounds that interacted with the PLpro key catalytic residues will be considered for further studies.

2.4. Molecular dynamics simulation

Molecular dynamics (MD) simulations of the protein and protein-ligand complexes were performed with a GROMACS 5.0 package [22], using Amber99SB force field and TIP3P water mode, under periodic boundary conditions with a dodecahedron periodic box set at a minimum distance of 1.0 between the protein and edge of the box. The system was neutralized with 0.154 moles/liter NaCl. The initial energy minimization process was conducted by applying a simulated annealing method with a corresponding equilibration of 1ns NVT and 1ns NPT. MD simulation production was performed at a constant temperature and pressure of 300 K and 1 atm, respectively, with a time step of 2 fs. The simulation was run in triplicate for 100 ns. Root mean square deviation (RMSD) and root mean square fluctuation (RMSF) were calculated to determine the stability of the protein-ligand complex [23].

2.5. Binding free-energy calculations using MMPBSA

The protein-ligand complexes' binding free energies (ΔG_{bind}) were computed using the Molecular Mechanics Poisson-Boltzmann Surface Area (MM-PBSA) algorithm, which gives a more accurate estimation of the free binding energy than the scoring function of docking experiments [24]. The GROMACS compatible g_mmpbsa tool package was used to implement the MM-PBSA

calculations, and the Python script MmPbSaStat.py provided in the g_mmpbsa package compiled and estimated the interaction free energies [25]. The total binding free energy (ΔG_{total}) is determined as the total energy released from the ligand-protein complex, which is contributed by molecular mechanics binding energy (ΔE_{MM}) and solvation free energy (ΔG_{sol}) using the following equations:

$$\Delta E_{MM} = \Delta E_{int} + \Delta E_{ele} + \Delta E_{vdw}$$

$$\Delta G_{sol} = \Delta G_{pl} + \Delta G_{np}$$

$$\Delta G_{total} = \Delta E_{MM} + \Delta G_{sol}$$

$$AG_{bind}\ (MM\text{-}PBSA) = \Delta E_{MM} + \Delta G_{sol} - \Delta T\Delta S$$

where ΔE_{int} stands for internal energy, ΔE_{ele} represents electrostatic energy, ΔE_{vdw} is for vander Waals energy, ΔG_{pl} is for polar energy, ΔG_{np} is for non-polar energy components, and ΔG_{sol} is the contribution to total solvation free energy, while ΔG_{bind} stands for the free energy of binding evaluated after entropic calculations $-\Delta T\Delta S$ [26].

2.6. ADMET analysis

SwissADME (www.swissadme.ch) and ADMETSAR (http://lmmd.ecust.edu.cn/admetsar2/) servers were employed to evaluate the metabolic and toxicological properties of the Ligands. The canonical format of the chemical compounds was used as the entry system for ADMET (absorption, distribution, metabolism and toxicity) calculations [27].

3. Results

3.1. Molecular docking

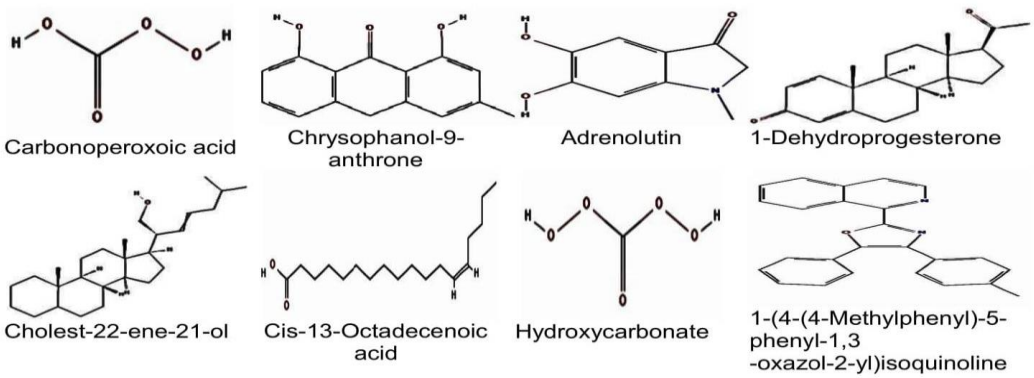

Figure1. Chemical structures of the identified ligands.

Table1. Binding scores and PLpro residues' interactions with the Ligands.

Compound Name	PubChem CID	Binding Score (kcal/mol)	Hydrogen Bond Interaction	Other Interactions
Carbonoperoxoic acid	181880	−4.4	**Asp 286**, Ile 285, Tyr 273	Leu 118, Thr 115, His 275, Ala 114, Trp 106, Lys 274, **Cys 111** and Gly 287
Chrysophanol-9-anthrone	68111	−6.7	Ser 212, Tyr 305, Glu 214	Glu 252, Tyr 251, Tyr 213, Thr 257 and Lys 254
Adrenolutin	12556	−5.9	His 175, Ala 153, Arg 82, Asn 156	His 73, Phe 79, Thr 74, Cys 155, Tyr 154 and Asp 76
1-Dehydroprogesterone	247929	−6.7	Lys 232	Leu 185, Thr 207, Met 208, Arg 166, Leu 199, Glu 203, Val 202, Ser 170 and Met 206
Cholest-22-ene-21-ol	129883894	−7.0	Ser 278	Thr 277, Lys 279, Gln 122, Gly 256, Thr 257, Tyr 305, Lys 217, Tyr 213, Lys 306, Thr 259 and Phe 258
Cis-13-Octadecenoic acid	5312441	−4.6	Asn 110, **Cys 111**	Gly 287, **Asp 286**, Asp 108, **His 272**, Asn 109, Ala 107, Ala 288, Lys 105, Trp 106, and Leu 289
Hydroxycarbonate	17887040	-4.5	His 275, Ile 285 and Ser 103	**Cys 111**, **Asp 286**, Tyr 273, Lys 274, Ala 114, Trp 106 and Thr 115
1-(4-(4-Methylphenyl) -5-phenyl-1,3 -oxazol-2-yl)isoquinoline	272358	−5.6	Trp 106	**Asp 286, His 272,** Lys 274, Lys 105, Thr 265 and Ala 288

Structural-based virtual screening was employed to find the potential inhibitors of SARS-CoV-2 PLpro. The docking and scoring functions were validated before the docking was carried out. Compounds that interacted with the catalytic site residues of PLpro were selected for further studies

(Figure 1). Carbonoperoxoic acid and hydroxycarbonate were identified from the PubChem similarity search of the *C. occidentalis* phytochemicals that bind to the active site, while 1-(4-(4-Methylphenyl)-5-phenyl-1,3-oxazol-2-yl)isoquinoline was identified from the NCI diversity set VI library, and the remaining five compounds are Cassia spp. phytochemicals.

The selected chemical compounds have binding scores ranging from −4.4 to 7.0 kcal/mol. Carbonoperoxoic acid, Chrysophanol-9-anthrone, Adrenolutin, 1-Dehydroprogesterone, Cholest-22-ene-21-ol, Cis-13-Octadecenoic acid, Hydroxycarbonateand1-(4-(4-Methylphenyl)-5-phenyl-1,3-oxazol-2-yl)isoquinoline showed binding scores of −4.4, −6.7, −5.9, −6.7, −7.0, −4.6, −4.5 and −5.6 kcal/mol, respectively (Table 1).

3.2. Analysis of the ligands' interactions

The 2D interactions of the eight selected ligands and the SARS CoV-2 PLpro complexes were visualized with the Discovery Studio software. As shown in Table 1 and Figure 2, carbonoperoxoic acid binds within the active site of SARS CoV-2 PLpro, forming hydrogen bonds with Asp 286, Ile 285 and Tyr 273 residues. It also formed hydrophobic interaction with Cys 111 and other active site residues, such as Leu 118, Thr 115, His 275, Ala 114, Trp 106, Lys 274 and Gly 287 (Figure 2a).

Chrysophanol-9-anthrone formed three hydrogen bonds with Ser 212, Tyr 305 and Glu 214 and hydrophobic bonds with Glu 252, Tyr 251, Tyr 213, Thr 257 and Lys 254 (Figure 2b).

Adrenolutin also interacted with His 175, Ala 153, Arg 82, Asn 156 through hydrogen bonds, with six other, hydrophobic bonds: His 73, Phe 79, Thr 74, Cys 155, Tyr 154 and Asp 76 (Figure 2c).1-Dehydroprogesterone formed only one hydrogen bond with Lys 232 and many other hydrophobic interactions with the nearby active site residues, such as Leu 185, Thr 207, Met 208, Arg 166, Leu 199, Glu 203, Val 202, Ser 170 and Met 206 (Figure 2d).

Cholest-22-ene-21-ol also forms only one hydrogen bond with Ser 278. It also interacts through hydrophobic bonding with Thr 277, Lys 279, Gln 122, Gly 256, Thr 257, Tyr 305, Lys 217, Tyr 213, Lys 306, Thr 259 and Phe 258 (Figure 2e).

Cis-13-Octadecenoic acid interacted with all the catalytic triads of SARS-CoV-2 PLpro. It forms a hydrogen bond with Cys 111 and hydrophobic interaction with Asp 286 and His 272. Others include an additional hydrogen bond with Asn 110 and hydrophobic interactions with Gly 287, Asp 108, Asn 109, Ala 107, Ala 288, Lys 105, Trp 106 and Leu 289 (Figure 2f). Because the structure of cis-13-Octadecenoic acid is long, a large part of the molecule is placed outside the active site and lies under the blocking loop 2 (BL2) in the palm sub-domain. Hydroxycarbonate forms three hydrogen bonds with His 275, Ser 103 and Ile 285 and vander Waals interactions with catalytic Cys111 and Asp 286.Other important interactions include Tyr 273, Lys 274, Trp 104 and Ala 114 (Figure 2g). On the other hand,1-(4-(4-Methylphenyl)-5-phenyl-1,3-oxazol-2-yl) isoquinoline forms a Pi-cation bond with Asp 286, Pi-anion bond with Lys 274 and Pi-donor hydrogen bond with Trp 106. Other significant interactions are His 272, Thr 265, Lys 105, Leu 289 and Ala 288 (Figure 2h).

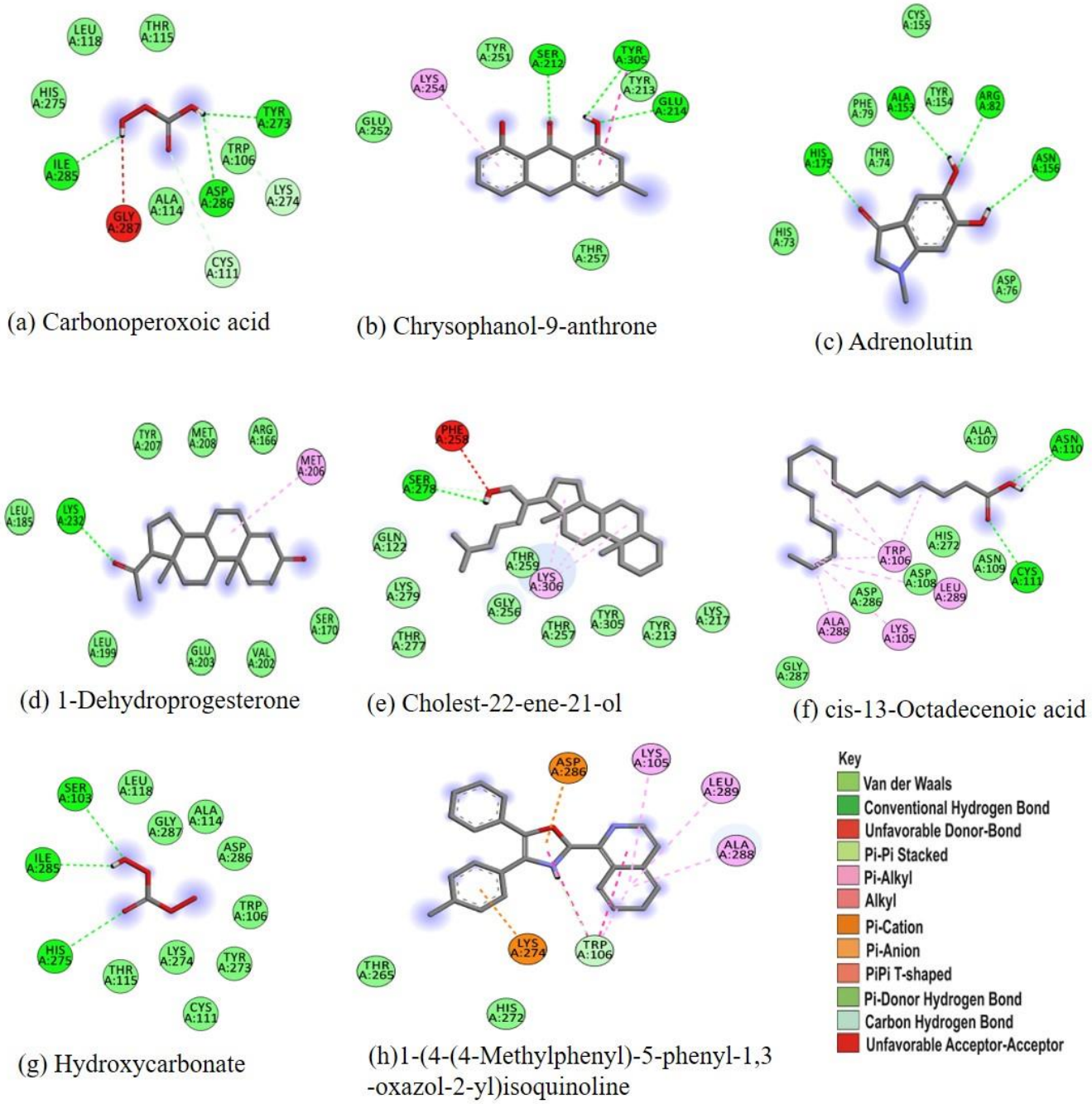

Figure 2. 2 D depiction of SARS-CoV-2 PLpro-*Ligands'* interactions complexes.

3.3. Molecular dynamics (MD) simulation

MD simulation is a widely used computational method for analyzing the ligand-protein complex dynamic behavior and stability under different conditions [23]. The simulation results were analyzed by RMSD and RMSF.

3.3.1. Root mean square deviation (RMSD)

The structural changes in protein-ligand complex and dynamic behavior were analyzed by the

RMSD and are presented in Figure 3.

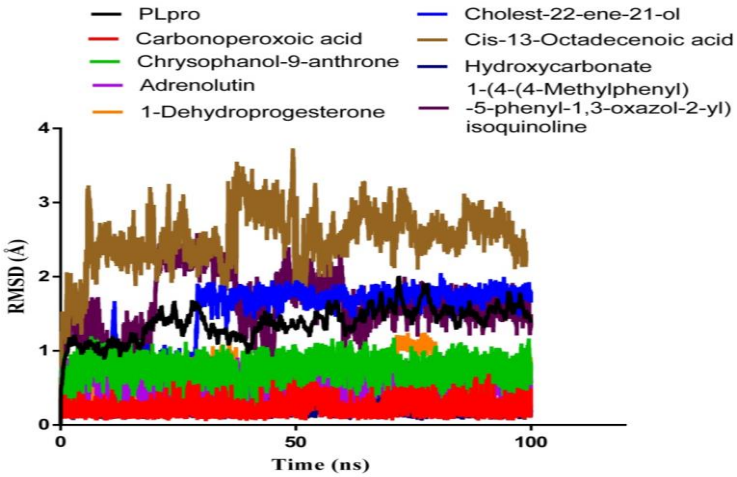

Figure 3. Plots of RMSD of the PLpro-ligands complex.

The results show that Carbonoperoxoic acid is highly stable at the active site of PLpro with a single binding mode; it fluctuates around 0.1 and 0.6 Å, with an average RMSD of 0.22 Å, which is even more stable than the Apo-protein. While Chrysophanol-9-anthrone reached stability at around 10 ns, it fluctuated between 0.2 and 1.2 Å, with an average RMSD of 0.75 Å. Adrenolutin is highly stable; it fluctuates around 0.6 Å throughout the simulation and has an average RMSD value of 0.62 Å.1-Dehydroprogesterone has two major fluctuations around 40 ns and 70 ns but becomes stable after 80 ns of the simulation. Similarly, Cholest-22-ene-21-ol becomes stable at around 30 ns following a large fluctuation at the beginning of the simulation, with an average RMSD of 1.43 Å. Cis-13-Octadecenoic acid remains stable but at a higher average RMSD that ranges between 2.06 and 3.55 Å and has a large fluctuation between 30 and 50 ns of the simulation. Hydroxycarbonate is also stable at the PLpro active site; it fluctuates between RMSD of 0.09 and 0.5 Å throughout the simulation, with an average RMSD value of 0.25 Å. 1-(4-(4-Methylphenyl)-5-phenyl-1,3-oxazol-2-yl)isoquinoline has two significant fluctuations between 16ns and 40ns and between 45 ns and 60 ns but stabilized from 60 ns till the end of the simulation.

3.3.2. Root mean square fluctuation (RMSF)

RMSF analysis was conducted to explore the per-residue fluctuations of the system. RMSF analysis showed that binding of the ligands does not affect the stability of the PLpro catalytic triad residues, Cys 111, Asp 286 and His 272 (Figure 4). The RMSF value of the Apo-protein reached equilibrium after an initial increase within the first 1ns, with an average RMSF of 1.2 Å.

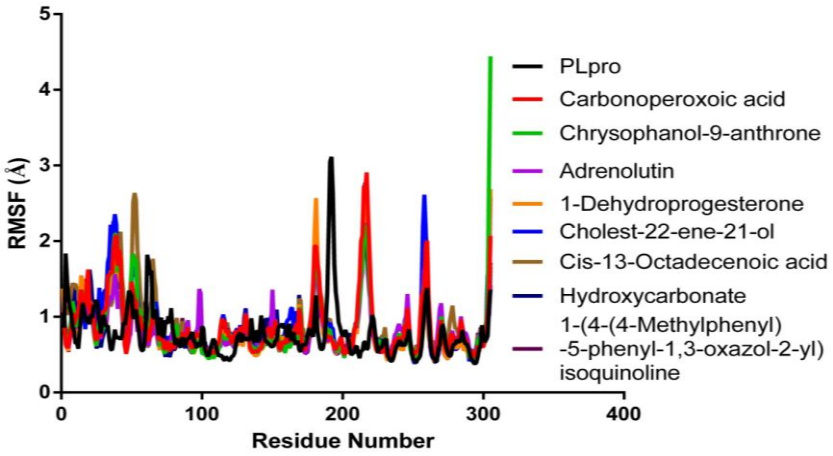

Figure 4. The root mean square fluctuation (RMSF).

As shown in Figure 4, the Apo-protein fluctuations during the simulation are shown in black color; its major fluctuations are at the residues from 66 to 75 (1.82 Å), 193 to 209 (2.1 Å) and 265 to 271 (1.41 Å). Carbonoperoxoic acid-PLPro complex, shown in red, has major fluctuations between residues 40 and 55 (2.03 Å), 183 and 196 (1.93 Å) and 264 and 271 (1.36 Å). Similarly, chrysophanol-9-anthrone-PLPro complex, shown in green, has fluctuations between 42 and 53 (2.09 Å), 189 and 193 (1.78 Å) and 219 and 230 (2.21 Å), similar to those of carbonoperoxoic acid. Adrenolutin-PLPro complex (purple) had major fluctuations between residues 43 and 50 (1.56 Å), 189 and 196 (1.77 Å) and 214 and 230 (2.21 Å). 1-dehydroprogesterone-PLPro complex (orange) causes fluctuations around residues 14 to 33 (1.55 Å), 41 to 55 (1.93 Å), 188 to 195 (2.57 Å) and 221 to 230 (2.75 Å). In contrast, Cholest-22-ene-21-ol-PLPro complex (represented in blue color) fluctuates at residues between 39 and 55 (2.36 Å), 189 and 192 (1.97 Å), 215 and 230 (2.46 Å) and 260 and 271 (2.62 Å), with an average RMSF higher than that of the Apo-protein. Cis-3-octadecenoic acid-PLPro complex (brown) major fluctuations are at the residues between 43 and 56 (2.13 Å), 59 and 67 (2.64 Å), 188 and 195 (1.86 Å) and 219 and 230 (2.69 Å). Hydroxycarbonate- PLPro complex (represented in navy blue) major fluctuations are between residues 36 and 55 (1.65 Å), 188 and 194 (1.67 Å), 222 and 230 (2.76 Å) and 264 and 271 (2.09 Å).1-(4-(4-Methylphenyl)-5-phenyl-1,3-oxazol-2-yl)isoquinoline-PLPro complex fluctuates around residues 42 to 53 (2.26 Å), 189 to 193 (2.01 Å) and 218 to 235 (2.11 Å).

3.4. Binding free energy of the PLpro-ligands complex using MMPBSA

The binding free energy was calculated to understand more about the interactions between PLpro and the ligands.

Table 2. Binding free energy of the PLpro in complex with the ligands.

Ligand-PLpro Complex	Vander Waals Energy (kcal/mol)	Electrostatic Energy (kcal/mol)	Polar Solvation Energy (kcal/mol)	Apolar Energy (kcal/mol)	Total Binding Energy (kcal/mol)
Carbonoperoxoic acid	−10.70 ±1.81	−20.46 ± 2.50	20.60 ± 1.39	−2.17 ± 0.02	−12.73 ± 1.39
Chrysophanol-9-anthrone	−22.12 ± 1.41	−2.90 ± 1.66	16.49 ± 2.49	−2.36 ± 0.08	−10.89 ± 2.05
Adrenolutin	−12.73 ± 1.98	−13.59 ± 2.37	21.31 ± 1.39	−2.18 ± 0.14	−7.20 ± 1.48
1−dehydroprogesterone	−21.61 ± 1.92	−4.43 ± 1.66	12.26 ± 2.07	−2.47 ± 0.10	−16.25 ± 1.72
Cholest-22-ene-21-ol	−22.57 ± 2.00	−12.51 ± 2.09	19.15 ± 1.38	−2.90 ± 0.12	−19.00 ± 1.83
Cis-13-Octadecenoic acid	−7.76 ± 0.66	−28.89 ± 2.63	32.96 ± 2.81	−1.22 ± 0.09	−5.00 ± 0.92
Hydroxycarbonate	−12.75 ± 2.26	−24.00 ± 3.32	26.12 ± 2.23	−2.57 ± 0.06	−13.21 ± 1.61
1-(4-(4-Methylphenyl)-5-phenyl-1,3-oxazol-2-yl)isoquinoline	−17.62 ± 1.43	−2.62 ± 0.86	10.31 ± 1.67	−2.52 ± 0.11	−12.45 ± 1.77

As shown in Table 2, the binding energies of the eight complexes range from −19.00 kcal/mol to −5.00 kcal/mol. Overall, Cholest-22-ene-21-ol shows the highest binding energy, followed by 1-Dehydroprogesterone. In contrast, Cis-13-Octadecenoic acid has the least binding energy.

3.5. MMPBSA energy decomposition analysis of the residue-ligand interactions

Binding free energy decomposition analysis was conducted to gain insight into the residues' contributions to the whole system. The energy contribution for each residue is shown in Figure 5.

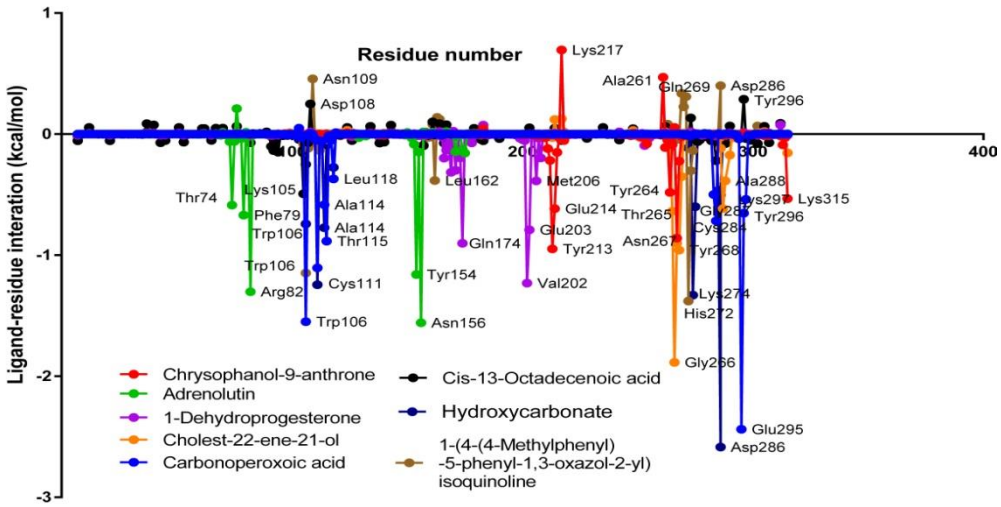

Figure 5. Energy spectra of the PLpro residues' interaction with the Ligands.

Notably, the energy contributions of the carbonoperoxoic acid-PLpro complex residues include catalytic Cys111(−1.104 kcal/mol), Tyr106(−1.549 kcal/mol), Thr115(−0.88 kcal/mol), Ala114(−0.58 kcal/mol), Leu118(−0.37 kcal/mol), Cys284(−0.72 kcal/mol), Tyr283(−0.49 kcal/mol), Glu295(−2.44 kcal/mol), Tyr296(−0.65 kcal/mol) and Lys297(−0.54 kcal/mol). Similarly, the major binding energy contributing residues in Chrysophanol-9-anthrone-PLpro complex are Tyr213(−0.95 kcal/mol), Glu214(−0.62 kcal/mol), Asn267(−0.86 kcal/mol), Tyr264(−0.48 kcal/mol), Tyr268(−0.22 kcal/mol) and Lys315(−0.53 kcal/mol). On the other hand, Lys217 and Ala261 binding energies were unfavorable. Adrenolutin–Plpro complex binding energy was contributed by Thr74 (−0.59 kcal/mol), Phe79 (−0.67 kcal/mol), Arg82 (−1.30 kcal/mol), Tyr154 (−1.16 kcal/mol) and Asn156 (−1.56 kcal/mol). Meanwhile, for1-dehydroprogesterone-PLpro complex, they are Gln174(−0.901 kcal/mol), Val202(−1.23 kcal/mol), Glu203(−0.79 kcal/mol) and Met206(−0.39 kcal/mol). Furthermore, Cholest-22-ene-21-ol-PLpro complex residues with obvious binding energy contributions are Gly266(−1.89 kcal/mol), Tyr268(−0.96 kcal/mol), Asn267(−0.90 kcal/mol), Thr265(−0.64 kcal/mol), Gln269(−0.35 kcal/mol), Gly288(−0.62 kcal/mol), Ala288(−0.39 kcal/mol) and Leu290(0.17 kcal/mol). Hydroxycarbonate-PLpro complex residues with enormous energy contributions are Try106(−0.74 kcal/mol), Cys111(−1.24 kcal/mol), Ala114(−0.77 kcal/mol), Leu118(−0.28 kcal/mol), Lys274(−1.33 kcal/mol), Asp286(−2.58 kcal/mol), Ile285(−0.46 kcal/mol), His272(0.11 kcal/mol), Asp286 (−0.50 kcal/mol) and His275(−0.6 kcal/mol). Finally,1-(4-(4-Methylphenyl)-5-phenyl-1,3-oxazol-2-yl)isoquinoline–Plpro complex binding energy contributing residues include Leu162(−1.38 kcal/mol) and Trp106(−0.30 kcal/mol), while Gln269,Asn109 and Asp286 have unfavorable binding energy.

3.6. Drug-likeness properties and ADMET screening

Table 3. Properties of the identified compounds.

Name	Log p	Log s	Rotatable bonds	Hydrogen bond acceptors	Hydrogen bond donors
Carbonoperoxoic acid	0.154	−0.07	1	4	2
Chrysophanol-9-anthrone	2.54142	−4.07	0	3	2
Adrenolutin	0.7303	−1.87	0	3	2
1-Dehydroprogesterone	4.4995	−4.28	1	2	0
Cholest-22-ene-21-ol	7.2462	−7.58	5	1	1
cis-13-Octadecenoic acid	6.1085	−5.41	15	2	1
Hydroxycarbonate	0.36	−0.67	2	5	2
1-(4-(4-Methylphenyl)-5-phenyl-1,3-oxazol-2-yl)isoquinoline	3.74	−6.32	3	3	0

Swiss ADME and admetSAR servers were used to evaluate the metabolic properties of the identified SARS CoV-2 PLpro inhibitors. As shown in Table 3, most of the compounds obeyed Lipinski rules for drug-likeness [28]. Carbonoperoxoic acid has a molecular weight of 78.02 g/mol, log P of 0.154, four hydrogen bond acceptors (HBA) and two hydrogen bond donors (HBD). Chrysophanol-9-anthrone compound has a molecular weight of 240.25 g/mol, log P of 2.54, three HBA and two HBD atoms. Adrenolutin has a molecular weight of 179.17 g/mol, log P of 0.73, log S

of −1.87, three HBA and two HBD. 1-Dehydroprogesterone has a molecular weight of 312.45 g/mol, log P of 4.49, log S of −4.28 and two HBA. Cholest-22-ene-21-ol has a molecular weight of 386.65 g/mol, log P of 7.25, log S of −7.58, 1 HBA and one HBD.Cis-13-Octadecenoic acid has a molecular weight of 282.46 g/mol, log P of 6.1, log S of −5.41, two HBA and one HBD. Hydroxycarbonate has a molecular weight of 9.402 g/mol,logP of 0.36, two Rotatable bonds, five HBA and two HBD. 1-(4-(4-Methylphenyl)-5-phenyl-1,3-oxazol-2-yl)isoquinoline has a molecular weight of 362.42 g/mol, logP of 3.74, three rotatable bonds, three HBA and Zero HBD.

Other Pharmacokinetic properties such as absorption, distribution, metabolism, excretion and toxicity are presented in Table 4. The identified ligands are readily absorbed by the human intestine, making them good candidates for oral administration. Meanwhile, only Chrysophanol-9-anthrone and 1-Dehydroprogesterone could pass through the Blood-brain barrier.

Table 4. ADMET of the identified compounds.

Absorption and distribution	Ligand 1	Ligand 2	Ligand 3	Ligand 4	Ligand 5	Ligand 6	Ligand 7	Ligand8
Water solubility	Very soluble	Moderately	Very soluble	Moderate	Poor	Moderate	Very soluble	Poorly soluble
Blood-brain barrier permeant	No	Yes	No	Yes	No	No	No	Yes
Human intestinal absorption	High	High	High	High	High	High	High	High
CNS permeability	No	No	No	No	No	No	No	No
P-glycoprotein I inhibitor	No	No	No	Yes	Yes	No	No	No
P-glycoprotein II inhibitor	No	No	No	No	Yes	No	No	No
Metabolism								
CYP450 2C9 inhibitors	No	No	No	yes	No	No	No	No
CYP450 2D6 inhibitors	No	No	No	No	No	No	No	No
CYP450 3A4 substrate	No	No	No	yes	Yes	yes	No	Yes
CYP450 1A2 substrate	No	yes	No	No	No	yes	No	Yes
CYP450 2C19 inhibitors	No	yes	No	No	No	No	No	Yes

Continued on next page

Toxicity								
AMES toxicity	No	No	No	No	No	No	No	No
hERG I inhibitor	No	No	No	No	No	No	No	No
hERG II inhibitor	No	No	No	Yes	Yes	No	No	No
Hepatotoxicity	No	No	No	Yes	No	Yes	No	No

Note:Ligand 1:Carbonoperoxoic acid, Ligand 2: Chrysophanol-9-anthrone, Ligand 3: Adrenolutin, Ligand 4:1-dehydroprogesterone, Ligand 5: Cholest-22-ene-21-ol, Ligand 6:cis-13-Octadecenoate acid, Ligand 7:Hydroxycarbonate, Ligand 8:1-(4-(4-Methylphenyl)-5-phenyl-1,3-oxazol-2-yl)isoquinoline.

4. Discussion

With the recent advancement in computational chemistry, chemical libraries could be screened for compounds with the potential to be utilized for drug development [17,29]. Several researchers have screened various chemical libraries in an attempt to discover potent PLpro inhibitors [15,16]. PLpro plays an essential role in the cleavage and maturation of SARS-CoV-2 poly-proteins, assembly of the replicase-transcriptase complex and disruption of host responses. The enzyme performs its proteolytic functions through its catalytic cysteine-protease cycle, in which Cys111 functions as a nucleophile, His272 acts as a general acid/base, and Asp286, linked with the histidine, assists to align and deprotonate Cys111 [5,6]. Several important structural features dictate access to the PLpro narrow active site, including a series of loops surrounding the area. One such loop is situated at the active site's mouth and comprises residues 103–110 [30]. As such, it is difficult for chemical compounds to fit the active site of SARS-CoV-2 PLpro. However, our study revealed that some of the identified compounds have the potential to bind to the SARS-CoV-2 PLpro catalytic triad and form crucial hydrogen bonds with catalytically essential residues of the enzyme and possibly inhibit its catalytic activity. For instance, carbonoperoxoic acid, cis-13-Octadecenoic acid, Hydroxycarbonate and 1-(4-(4-Methylphenyl)-5-phenyl-1,3-oxazol-2-yl)isoquinoline interacted with at least one of the active site catalytic triad residues of SARS-CoV-2 PLpro. More importantly, hydrogen bonds were formed between Carbonoperoxoic acid and Asp286, Ile285 and Tyr 273, while cis-13-Octadecenoic acid formed hydrogen bonds with Cys111 and Asn110. Hydroxycarbonate forms three hydrogen bonds with His 275, Ser 103 and Ile 285, and van der Waals interactions with catalytic Cys111 and Asp286. On the other hand, 1-(4-(4-Methylphenyl)-5-phenyl-1,3-oxazol-2-yl) isoquinoline forms a Pi-cation bond with Asp 286, Pi-anion bond with Lys 274 and Pi-donor hydrogen bond with Trp 106, which are all critical for the enzyme activity. On the other hand, adrenolutin binds to the pocket in the ubiquitin-binding domain and forms key hydrogen bonds with His 175, Ala 153, Arg 82 and Asn 156. Recent in-vitro studies imply that PLpro inhibitors that bind to the active or ubiquitin-binding sites are promising candidates for drug development [6]. In similar studies, Debnath *etal.* identified myricetin from *Allium cepa* and α-hydroxy-hydro-caffeic acid from *Mentha piperita*, both of which interacted with the SARS-Cov-2 PLpro [31].

Furthermore, several new molecules with anti-Covid-19 properties were identified by in silico studies, most of which are comparable to our findings. For instance, Hajbabaie *etal.* conducted a virtual screening of more than 300 thousand ligands and identified two compounds with binding

scores of −9.4 and −9.36 kcal/mol which interacted with Asp 164, Glu 269, Tyr 264 and Tyr 268. Similarly, a known PLpro inhibitor GLR0617 binds to the cavity near catalytic residues and induces the blockage of loop2, thereby preventing catalysis as observed in adrenolutin interaction[16]. An in-vitro study confirmed that a naphthalene-based compound identified by in silico studies has anti-PLpro activity [15]. Likewise, through virtual screening and enzymatic evaluations, nine natural biflavones were confirmed to be effective PLpro inhibitors with IC50 values ranging from 9.5 to 43.2 μM [32]. Adam *etal.* identified a compound that formed a hydrogen bond with Gly 163 and Alkyl interaction with Cys 111 and Leu 162 [33].

In our study, molecular dynamics simulation revealed that all the selected compounds formed a stable complex with SARS-CoV-2 PLpro. Similarly, MMPBSA revealed significant binding energies of the complexes. Cholest-22-ene-21-ol showed the highest binding energy, followed by 1-Dehydroprogesterone, while Cis-13-Octadecenoic acid has the least binding energy.

Metabolic and toxicity studies show that the identified compounds were all soluble and highly absorbed through the human intestine. Only Chrysophanol-9-anthrone and1-Dehydro progesterone are permeable to the blood-brain barrier (Table 4). Several studies revealed the therapeutic potential of the identified chemical compounds. For instance, Chrysophanol, which is a unique anthraquinone, has broad-spectrum therapeutic potential. It has been reported to possess anticancer, antiviral, anti-diabetic, anti-inflammatory and anti-protozoal effects [17]. Cholest-22-ene-21-ol has been reported to have an anti-inflammatory effect [34].Cis-13-octadecenoic acid is used for therapeutic uses in medicine and surgery [35], and Hydroxycarbonate is used in the synthesis of iron-magnesium-hydroxycarbonate for the treatment of hyperphosphatemia [36]. 1-(4-(4-Methylphenyl)-5-phenyl-1,3-oxazol-2-yl)isoquinoline modulates signal transduction through the Pd-1 receptor, which activates t-cells to promote immune response for treating infections, as reported in PubChem bioassay result.

5. Conclusions

Covid-19 remains the most significant challenge facing the world today, and so far, there is no standard therapeutic for its management. PLpro plays a critical role in viral replication and pathogenesis. Our present study has identified eight compounds, some of which form bonds with at least one of the catalytic triads of the PLpro, which is often difficult to achieve due to the presence of critical structural features that dictate access to the PLpro narrow active site. These ligands might have antiviral properties and the capacity to be promising drug candidates for the treatment of Covid-19. Furthermore, these compounds warrant further lead optimization and in-vitro studies.

Conflict of interest

The authors declare no conflict of interest.

Author contributions

MM, IYH and DL: conceptualization, methodology, writing of the original draft, editing and reviewing; AY, AJA and SYI: writing of the original draft, methodology; TAM, AJ and HS: methodology and writing of the original draft. All authors have read and approved the manuscript.

References

1. Hilgenfeld R (2014) From SARS to MERS: crystallographic studies on coronaviral proteases enable antiviral drug design. *FEBS J* 18: 4085–4096. https://doi.org/10.1111/febs.12936
2. Singhal T (2020) A review of coronavirus disease-2019 (COVID-19). *Indian J Pediatr* 87: 281–286. https://doi.org/10.1007/s12098-020-03263-6
3. Aftab SO, Ghouri MZ, Masood MU, et al. (2020) Analysis of SARS-CoV-2 RNA-dependent RNA polymerase as a potential therapeutic drug target using a computational approach. *J Transl Med* 18: 275. https://doi.org/10.1186/s12967-020-02439-0
4. ul Qamar MT, Alqahtani SM, Alamri MA, et al. (2020) Structural basis of SARS-CoV-2 3CLpro and anti-COVID-19 drug discovery from medicinal plants. *J Pharm Anal* 10: 313–319. https://doi.org/10.1016/j.jpha.2020.03.009
5. Gao X, Qin B, Chen P, et al. (2021) Crystal structure of SARS-CoV-2 papain-like protease. *Acta Pharm Sin B* 11: 237–245. https://doi.org/10.1016/j.apsb.2020.08.014
6. Osipiuk J, Azizi SA, Dvorkin S, et al. (2021) Structure of papain-like protease from SARS-CoV-2 and its complexes with non-covalent inhibitors. *Nat Commun* 12: 743. https://doi.org/10.1038/s41467-021-21060-3
7. Mielech AM, Chen Y, Mesecar AD, et al. (2014) Nidovirus papain-like proteases: multifunctional enzymes with protease, deubiquitinating and deISGylating activities. *Virus Res* 194: 184–190. https://doi.org/10.1016/j.virusres.2014.01.025
8. Lindner HA, Lytvyn V, Qi H, et al. (2007) Selectivity in ISG15 and ubiquitin recognition by the SARS coronavirus papain-like protease. *Arch Biochem Biophys* 466: 8–14. https://doi.org/10.1016/j.abb.2007.07.006
9. Swaim CD, Canadeo LA, Monte KJ, et al. (2020) Modulation of extracellular ISG15 signaling by pathogens and viral effector proteins. *Cell Rep* 31: 107772. https://doi.org/10.1016/j.celrep.2020.107772
10. Barretto N, Jukneliene D, Ratia K, et al. (2005) The papain-like protease of severe acute respiratory syndrome coronavirus has deubiquitinating activity. *J Virol* 79: 15189–15198. https://doi.org/10.1128/JVI.79.24.15189-15198.2005
11. Klemm T, Ebert G, Calleja DJ, et al. (2020) Mechanism and inhibition of the papain-like protease, PLpro, of SARS-CoV-2. *EMBO J* 39: e106275. https://doi.org/10.15252/embj.2020106275
12. Chojnacka K, Witek-Krowiak A, Skrzypczak D, et al. (2020) Phytochemicals containing biologically active polyphenols as an effective agent against Covid-19-inducing coronavirus. *J Funct Foods* 73: 104146. https://doi.org/10.1016/j.jff.2020.104146
13. Alamri MA, Tahir Ul Qamar M, Mirza MU, et al. (2021) Pharmacoinformatics and molecular dynamics simulation studies reveal potential covalent and FDA-approved inhibitors of SARS-CoV-2 main protease 3CLpro. *J Biomol Struct Dyn* 39: 4936–4948. https://doi.org/10.1080/07391102.2020.1782768
14. Oladele JO, Adewole TS, Ogundepo GE, et al. (2022) Efficacy of selected Nigerian tropical plants in the treatment of COVID-19: in silico and in vitro investigations. *Environ Sci Pollut Res* 29: 627. https://doi.org/10.1007/s11356-022-22025-9

15. Yan F, Gao F (2021) An overview of potential inhibitors targeting non-structural proteins 3 (PLpro and Mac1) and 5 (3CLpro/Mpro) of SARS-CoV-2. *Comput Struct Biotechnol J* 19: 4868–4883. https://doi.org/10.1016/j.csbj.2021.08.036
16. Hajbabaie R, Harper MT, Rahman T (2021) Establishing an analogue based in silico pipeline in the pursuit of novel inhibitory scaffolds against the SARS coronavirus 2 papain-like protease. *Molecules* 26: 1134. https://doi.org/10.3390/molecules26041134
17. Yadav JP, Arya V, Yadav S, et al. (2010) Cassia occidentalis L.: a review on its ethnobotany, phytochemical and pharmacological profile. *Fitoterapia* 81: 223–230. https://doi.org/10.1016/j.fitote.2009.09.008
18. Socrates SH, Mohan SC (2019) Phytochemical analysis of flower extracts of different Cassia species by using gas chromatography-mass spectrometry. *Int J Biol Chem* 13: 1–11.
19. Manikandaselvi S, Vadivel V, Brindha P, et al. (2016) Studies on physicochemical and nutritional properties of aerial parts of Cassia occidentalis L. *J Food Drug Anal* 24: 508–515. https://doi.org/10.1016/j.jfda.2016.02.003
20. Mirza MU, Froeyen M (2020) Structural elucidation of SARS-CoV-2 vital proteins: Computational methods reveal potential drug candidates against main protease, Nsp12 polymerase and Nsp13 helicase. *J Pharm Anal* 10: 320–328. https://doi.org/10.1016/j.jpha.2020.04.008
21. Pettersen EF, Goddard TD, Huang CC, et al. (2004) UCSF Chimera—a visualization system for exploratory research and analysis. *J Comput Chem* 25: 1605–1612. https://doi.org/10.1002/jcc.20084
22. Pronk S, Páll S, Schulz R, et al. (2013) GROMACS 4.5: a high-throughput and highly parallel open source molecular simulation toolkit. *Bioinformatics* 29: 845–854. https://doi.org/10.1093/bioinformatics/btt055
23. Vanommeslaeghe K, Hatcher E, Acharya C, et al. (2010) CHARMM general force field: a force field for drug-like molecules compatible with the CHARMM all-atom additive biological force fields. *J Comput Chem* 31: 671–690. https://doi.org/10.1002/jcc.21367
24. Genheden S, Ryde U (2015) The MM/PBSA and MM/GBSA methods to estimate ligand-binding affinities. *Expert Opin Drug Discov* 10: 449–461. https://doi.org/10.1517/17460441.2015.1032936
25. Kumari R, Kumar R, Consortium OSDD, et al. (2014) g_mmpbsa–A GROMACS tool for high-throughput MM-PBSA calculations. *J Chem Inf Model* 54: 1951–1962. https://doi.org/10.1021/ci500020m
26. Miller III BR, McGee Jr TD, Swails JM, et al. (2012) MMPBSA. py: an efficient program for end-state free energy calculations. *J Chem Theory Comput* 8: 3314–3321. https://doi.org/10.1021/ct300418h
27. Cheng F, Li W, Zhou Y, et al. (2012) admetSAR: a comprehensive source and free tool for assessment of chemical ADMET properties. *J Chem Inf Model* 52: 3099–3105. https://doi.org/10.1021/ci300367a
28. Ntie-Kang F (2013) An in silico evaluation of the ADMET profile of the StreptomeDB database. *Springerplus* 2: 353. https://doi.org/10.1186/2193-1801-2-353
29. Sofowora A, Ogunbodede E, Onayade A, et al. (2013) The role and place of medicinal plants in the strategies for disease prevention. *Afr J Tradit Complement Altern Med* 10: 210–229. https://doi.org/10.4314/ajtcam.v10i5.2

30. Ratia K, Saikatendu KS, Santarsiero BD, et al. (2006) Severe acute respiratory syndrome coronavirus papain-like protease: structure of a viral deubiquitinating enzyme. *Proc Natl Acad Sci* 103: 5717–5722. https://doi.org/10.1073/pnas.0510851103
31. Debnath B, Debnath P, Ghosh R, et al. (2021) In silico identification of potential inhibitors of SARS-CoV-2 papain-like protease from natural sources: A natural weapon to fight COVID-19. *Coronaviruses* 2: 16–27. https://doi.org/10.2174/2666796701999201203211330
32. Li L, Ma L, Hu Y, et al. (2022) Natural biflavones are potent inhibitors against SARS-CoV-2 papain-like protease. *Phytochemistry* 193: 112984. https://doi.org/10.1016/j.phytochem.2021.112984
33. Stasiulewicz A, Maksymiuk AW, Nguyen ML, et al. (2021) SARS-CoV-2 papain-like protease potential inhibitors—in silico quantitative assessment. *Int J Mol Sci* 22: 3957. https://doi.org/10.3390/ijms22083957
34. Johnson TO, Odoh KD, Nwonuma CO, et al. (2020) Biochemical evaluation and molecular docking assessment of the anti-inflammatory potential of Phyllanthus nivosus leaf against ulcerative colitis. *Heliyon* 6: e03893. https://doi.org/10.1016/j.heliyon.2020.e03893
35. Astiti NPA, Ramona Y (2021) GC-MS analysis of active and applicable compounds in methanol extract of sweet star fruit (Averrhoa carambola L.) leaves. *HAYATI J Biosci* 28: 12–12. https://doi.org/10.4308/hjb.28.1.12
36. McIntyre CW, Pai P, Warwick G, et al. (2009) Iron-magnesium hydroxycarbonate (fermagate): a novel non-calcium-containing phosphate binder for the treatment of hyperphosphatemia in chronic hemodialysis patients. *Clin J Am Soc Nephrol* 4: 401–409. https://doi.org/10.2215/CJN.02630608

AIMS Press